MORPHOLOGICAL TEXTURE DESCRIPTION FOR HYPERSPECTRAL IMAGES: PATTERN SPECTRUM

H. Deborah

Norwegian University of Science and Technology
Department of Computer Science
Teknologivn. 22, Gjøvik, Norway

N. Richard

University of Poitiers
Laboratory XLIM, JRU CNRS 7252
Futuroscope Chasseneuil Cedex, France

ABSTRACT

A metrological extension of morphological granulometry for the hyperspectral domain is introduced in this work. This development is enabled by the latest study of a suitable ordering relation for hyperspectral images. With granulometry as a texture descriptor, a suitable similarity measure for it is also introduced. In addition to providing validation experiments to the extension, a preliminary result in a texture discrimination task can also be found in this work.

***Index Terms*—** Texture, mathematical morphology, pattern spectrum, hyperspectral

1. INTRODUCTION

Mathematical morphology (MM) offers a framework of theory and tools for the analysis of spatial structures in an image. It has been widely known mostly for its elementary operators, e.g., erosion-dilation and opening-closing pairs, or segmentation tools, e.g., watershed and skeletonization. While they are useful and can be found at the core of many image processing and analysis solutions [1, 2, 3], MM also provides a set of tools capable of dealing with textures such as *granulometry* or, its derivative form, *pattern spectrum* [4].

Granulometry provides information on the distributions of object size and distance in an image. The important advantage of granulometry is that it requires no segmentation step, making the processing an efficient one. Finally, pattern spectrum can be used as a descriptor for texture images.

This article is organized as follows. The extension of morphological granulometry to the hyperspectral domain is introduced in Sec. 2. In Sec. 3, a validation experiment is provided, showing also how a pattern spectrum is interpreted. Then, in Sec. 4, a demonstration of its use in a texture discrimination task is given. A suitable texture similarity measure for pattern spectrum is also introduced. Finally, the work is concluded in Sec. 5. Table 1 is provided for easy access to frequently used mathematical notations.

This work is supported by FRIPRO FRINATEK Metrological texture analysis for hyperspectral images (projectnr. 274881) funded by the Research Council of Norway.

2. MORPHOLOGICAL GRANULOMETRY

In material science, granulometry is the measurement of the distribution of size in a collection of grains. In mining, the measurement can be carried out by the sieving of grains or particles with increasing mesh size. At each increment, the mass of grains retained in the sieve will be then recorded.

2.1. Definition

The physical process of sieving grains with increasing mesh size is analogous to successively applying morphological opening (or, its dual, *closing*) operations with increasing structuring element size [4]. After each opening, the volume of the resulting image is computed as follows:

$$\nu(\gamma_{B_i}(I)) = \int \gamma_{B_i}(I),\ i \in [1, r] \tag{1}$$

A granulometric curve can therefore be obtained as a function of structuring element size. *Pattern spectrum* (PS) is a derivative of the granulometric curve where, instead of recording volume evolution, it is the loss of volume at each succession that is calculated:

$$\nu(\gamma_{B_i}(I)) - \nu(\gamma_{B_{i-1}}(I)),\ i \in [1, r] \tag{2}$$

Compared to the granulometric curve, PS can be regarded as more intuitive since the location of its peak directly refers to the dominant or prevalent size occurring in the image.

2.2. Theoretical requirements

Since granulometry is obtained through a series of opening, the theoretical properties of an opening is also obtained, i.e., *anti-extensivity*, *increasingness*, and *idempotence*. Additionally, granulometry also posseses a property that is stronger than idempotence, i.e., *absorption* [4]. Idempotence expresses that multiple openings applied to an image will not modify the image further, given that the structuring element size remains the same:

$$\gamma_B(I) = \gamma_B(\gamma_B(I)).$$

Table 1: Frequently used mathematical notations.

S	A spectrum as a function of wavelength
λ	Wavelength, $\lambda \in [\lambda_{\min}, \lambda_{\max}]$
I, I^n	Grayscale and n-dimensional image functions, respectively
$\preceq, \succeq$	Logical ordering relation "less than or equal to" and "greater than or equal to", respectively
$d(S_1, S_2)$	Distance between S_1 and S_2
$S^{-\infty}$, $S^{+\infty}$	Spectral references associated to minimum and maximum rank extraction, respectively
γ, ϕ	Opening and closing operations, respectively
B_i	Structuring element of arbitrary size i
ν	Image volume

With the absorption property, applying a series of opening with increasing structuring element size is equal to applying only the opening with the largest size:

$$\gamma_{B_i}(\gamma_{B_j}(I)) = \gamma_{B_j}(\gamma_{B_i}(I)) = \gamma_{\max(B_i,B_j)}(I).$$

As a note, the absorption property is not automatically obtained. It is also dependent upon the choice of the structuring element shape, i.e., only satisfiable through periodic lines and disks [4]. However, there are more issues to address due to the digital approximation of disks [5, 6]. In this work, we decide to work only with square and diamond structuring elements to avoid bias that is caused by the digital reconstruction of disks.

2.3. Extension to the hyperspectral domain

The initial formulation of granulometry is developed for binary and gray level images, where the distinction between object and background is straightforward. Its extension to the hyperspectral domain requires a suitable ordering function.

2.3.1. *Ordering relation*

The first and most fundamental challenge in the extension of MM to any multivariate domain is the ordering relation. This is because, at the center of its processing, MM requires determining the minimum and maximum values of a set of pixel values contained by the structuring element. In this work, we will use the *conditional ratio and angular* (CRA) ordering relation, which has been shown to be the most suitable for hyperspectral image processing in a previous study, respecting, in addition, the expected metrological properties [7].

CRA, as given in (3), is an ordering relation developed based on the ratio of distances relative to two spectral references $S^{-\infty}$ and $S^{+\infty}$. The first and second conditions are ratios of distances proportional to magnitude and shape differences between two spectra, respectively. Distance function d used throughout this work is the Kullback-Leibler pseudo-divergence (KLPD) function [8], whose performance has been evaluated and compared in Ref. [9].

$$\begin{aligned} S_1 \preceq S_2 \Leftrightarrow &\begin{cases} R_0(S_1) > R_0(S_2) \text{ or} \\ R_0(S_1) = R_0(S_2) \text{ and } R_2(S_1) < R_2(S_2) \end{cases} \\ S_1 \succeq S_2 \Leftrightarrow &\begin{cases} R_1(S_1) > R_1(S_2) \text{ or} \\ R_1(S_1) = R_1(S_2) \text{ and } R_2(S_1) > R_2(S_2) \end{cases} \\ \text{where } R_0 = &\frac{d(S_i, S^{+\infty})}{d(S_i, S^{-\infty})},\ R_1 = \frac{d(S_i, S^{-\infty})}{d(S_i, S^{+\infty})}, \text{ and} \\ R_2 = &\frac{2 \cdot d(S_i, S^{-\infty})}{d(S^{-\infty}, S^{+\infty})}. \end{aligned} \tag{3}$$

2.3.2. *Image volume*

The next challenge to tackle lies in adapting (1) to the hyperspectral domain. For a grayscale image, the use of a single integral is sufficient and appropriate since the image can be regarded as topology. The volume is essentially the gray area bounded by the image plane I and the spatial support of the image (or, the plane at zero value), see Fig. 1a.

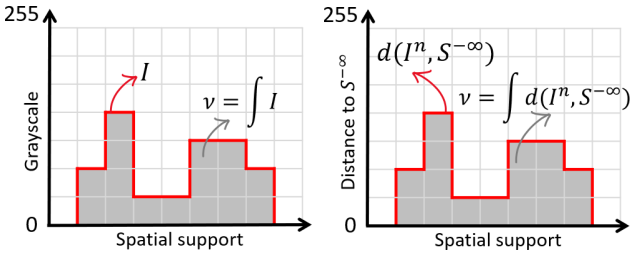

Fig. 1: Illustration of the computation image volume in the (a) grayscale domain and (b) spectral difference space.

In the hyperspectral domain, the pixel values are n-dimensional. Thus, the image function is not describable as a plane but rather in an (n+1)-dimensional space, with n equals the numbers of spectral bands. To reduce the problem into a two-dimensional space, in this work, the image volume is considered in a spectral difference space:

$$\nu(\gamma_{B_i}(I^n)) = \int\int d(\gamma_{B_i}(I^n), S^{-\infty}) dx\ dy, \tag{4}$$

where $i \in [1, r]$, and x and y are the axes of the spatial support. Essentially, given a reference spectrum $S^{-\infty}$ with the same spectral dimension as the opening result $\gamma_{B_i}(I^n)$, we can obtain a spectral difference plane relative to $S^{-\infty}$. In this way, we are also defining the plane at zero distance values, i.e., where $S^{-\infty}$ is located. See illustration in Fig. 1b.

3. VALIDATION EXPERIMENT

Based on the knowledge that a PS provides information of the distribution of shape and size in an image, a set of hyperspectral images as shown in Fig. 2 are generated. Each image consists of a background and 16 square objects as foreground.

3.1. Binary pseudo-artificial test case

The first dataset (Fig. 2) is composed of binary spectral images. They are constructed using only two spectra, associated with each pixel location using a binary mask. Their PS are expected to be identical to the theory for binary images.

PS obtained for the set of varying pattern size and distance can be seen in Fig. 3. The left side of each plot is obtained by opening and corresponds to the distance between the square patterns. Obtained by closing, the right side provides complementary information regarding the size of the patterns. The peak locations are directly related to the pattern size or distance n through the function $n + 2$.

The magnitude of the peaks in a PS is partly related to the contrast between the pattern and the background. In this second experiment, we are assessing the performance of PS in a more realistic case. The same binary mask is used, but the background and pattern content are extracted from hyperspectral images of real physical objects, see Fig. 4.

(a) Varying square widths (5, 10, 15, 20, 25) and fixed distance of 20 pixels

(b) Fixed square width of 15 pixels and varying distance (4, 8, 12, 16, 20)

Fig. 2: Binary test set with varying pattern size and distance. The same two spectra are used to create the background and foreground parts for all images.

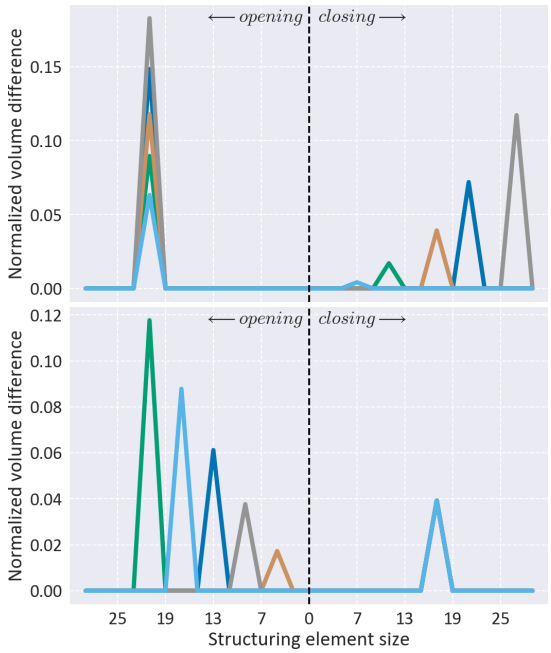

Fig. 3: Pattern spectra obtained for binary test sets with variations in **(top)** pattern size and **(bottom)** pattern distance.

3.2. Textured pseudo-artificial dataset

Fig. 5 shows the obtained PS for the second dataset. Peak locations in these plots are related to the pattern size and distance. It can also be observed that aside from the peaks, the spectra are mostly related to that of the background (BG). PS content of the foreground patterns is also present albeit not visible since its statistical representation area is weak.

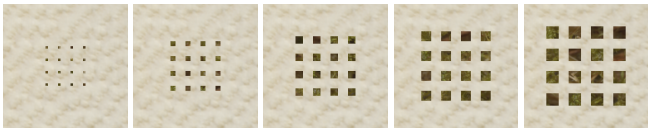

(a) Varying square widths (5, 10, 15, 20, 25) and fixed distance of 20 pixels

(b) Fixed square width of 15 pixels and varying distance (4, 8, 12, 16, 20)

Fig. 4: Textured test set with varying pattern size and distance. Background and foreground contents are extracted from hyperspectral images of real objects.

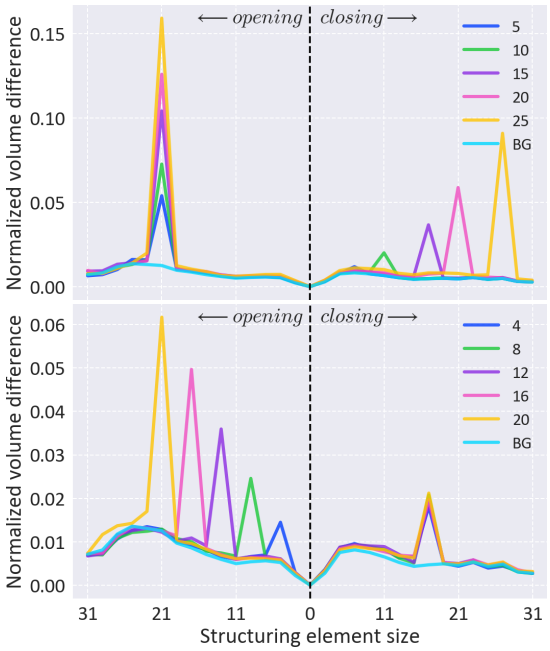

Fig. 5: Pattern spectra obtained for textured test sets in Fig. 4, with variations in **(top)** pattern size and **(bottom)** distance.

4. SIMILARITY ASSESSMENT BETWEEN PATTERN SPECTRA

The initial writing of granulometry was defined for binary images [11]. In this context, PS can be transformed into a probability density function (PDF) of the coverage of a surface by objects, each a product of its frequency and size. The extension of granulometry to the grayscale and multivariate domains loses this direct metrological relationship. It is because the product of object coverage and contrast to the background is computed together in a single integral as in (1). Consequently, a PS is not a PDF and must rather be considered as a sampled function of a complex granulometry due to its absorption property. Considering it as a texture descriptor, a texture similarity measure is required to carry out texture discrimination tasks. Since a PS is not a PDF, similarity functions defined for PDFs are therefore not suitable [12]. Based on these considerations, KLPD function [8] is selected to measure the difference between two PS.

To demonstrate the use of PS descriptor and KLPD function in a texture discrimination task, 10 images shown in Fig. 6 are employed as experiment target. Their obtained PS are provided in Fig. 7. Through visual observation, the texture of **chili** and **milkcoffee** images are quite similar. Their corresponding PS are also similar in terms of shape, but quite different in magnitudes. But this is as expected since the magnitude of a PS is also linked to the image contrast. Note that in the spectral domain, the discussion around image contrast becomes a question of spectral variations within an image. Among all PS, one that corresponds to the **rice** image has a very different trend compared to the rest, with a significant opening-peak at a large structuring element radius. This reflects the prominent object size in the image. If we look at the PS of **tea-02-biloba**, it also has a peak at a similar location. However, since the image consists of objects of various sizes, this peak is not as significant as that of the **rice**.

The difference between each pair of these texture images is also computed and shown as a heatmap in Fig. 8. In addition to confirming the previous observations, this heatmap allows us to observe the granulometric variations within this dataset. The image **rice** can be said as quite different from most of the other images. The highest differences can be seen for the pairs of **chili-tea-04**, **chili-oregan**, and **pepper-rice**. We also need to note that PS is relative to the local variations and does not embed the first-order statistics, i.e., the distribution of spectra. Therefore, the difference map is not relative to the average color differences but rather is restricted to texture variations.

5. CONCLUSION

In this work, we have introduced a metrological extension of morphological granulometry to the spectral domain. This extension is possible due to the latest development of the *conditional ratio and angular* ordering relation for hyperspectral images. Considering granulometry as a texture descriptor, we paired it with a suitable similarity measure, i.e., Kullback Leibler pseudo-divergence. A demonstration of their performance in a texture discrimination task was also provided, using a texture database available for the hyperspectral domain.

6. SUPPLEMENTARY MATERIALS

Images from the binary and textured test sets are available via `doi.org/10.5281/zenodo.3709776`.

Fig. 6: Subsets (512×512 pixels) of Hytexila image database of **food** category [10].

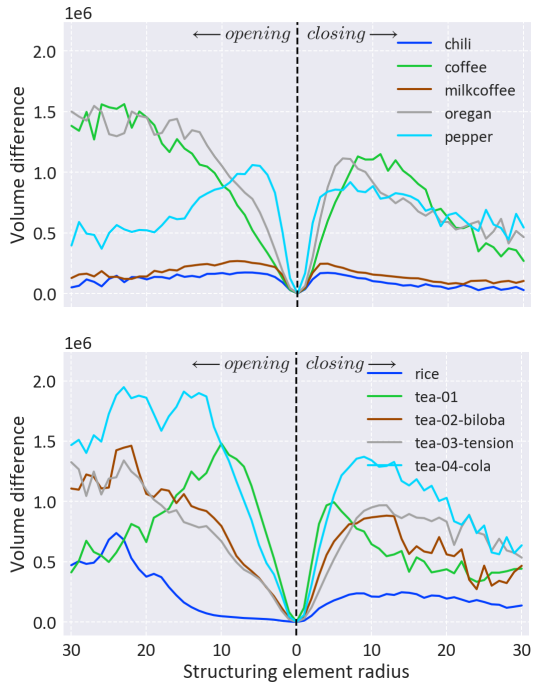

Fig. 7: Pattern spectra of hytexila-food shown in Fig. 6. Note that x-axes of both plots are identical.

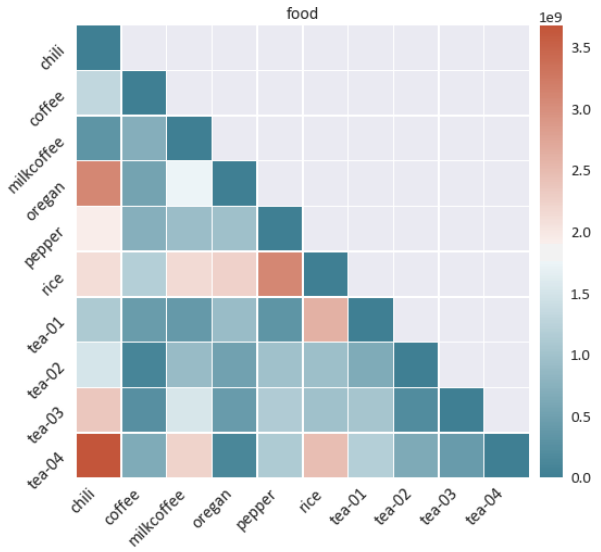

Fig. 8: Difference matrix of pattern spectra shown in Fig. 7, presented as a heatmap.

7. REFERENCES

[1] Y. Yang, M. Yang, S. Huang, Y. Que, M. Ding, and J. Sun, "Multifocus image fusion based on extreme learning machine and human visual system," *IEEE Access*, vol. 5, pp. 6989–7000, 2017.

[2] S. Liu, L. Dong, X. Liao, Y. Hao, X. Cao, and X. Wang, "A dilation and erosion-based clustering approach for fault diagnosis of photovoltaic arrays," *IEEE Sens J*, vol. 19, no. 11, pp. 4123–4137, 2019.

[3] G. Boato, D. Dang-Nguyen, and F. G. B. De Natale, "Morphological filter detector for image forensics applications," *IEEE Access*, pp. 1–1, 2020.

[4] P. Soille, *Morphological Image Analysis: Principles and Applications*, Springer-Verlag New York, Inc., 2nd edition, 2003.

[5] R. Adams, "Radial decomposition of disks and spheres," *CVGIP: Graphical Models and Image Processing*, vol. 55, no. 5, pp. 325 – 332, 1993.

[6] A. Ledoux, *Vers des traitements morphologiques couleur et spectraux valides au sens perceptuel et physique: Méthodes et critères de sélection*, phdthesis, University of Poitiers, Dec 2013.

[7] H. Deborah, N. Richard, J. Y. Hardeberg, and C. Fernandez-Maloigne, "Assessment protocols and comparison of ordering relations for spectral image processing," *IEEE J Sel Top Appl Earth Obs Remote Sens*, vol. 11, no. 4, pp. 1253–1265, 2018.

[8] N. Richard, D. Helbert, C. Olivier, and M. Tamisier, "Pseudo-divergence and bidimensional histogram of spectral differences for hyperspectral image processing," *J Imaging Sci Technol*, vol. 60, no. 5, pp. 1–13, 2016.

[9] H. Deborah, *Towards Spectral Mathematical Morphology*, phdthesis, Norwegian University of Science and Technology, University of Poitiers, Dec 2016.

[10] H. A. Khan, S. Mihoubi, B. Mathon, J. B. Thomas, and J. Y. Hardeberg, "Hytexila: High resolution visible and near infrared hyperspectral texture images," *Sensors*, vol. 18, no. 2045, 2018.

[11] G. Matheron, *Eleménts pour une Théorie des Milieux Poreux*, Masson, 1967.

[12] H. Deborah, N. Richard, and J. Y. Hardeberg, "A comprehensive evaluation of spectral distance functions and metrics for hyperspectral image processing," *IEEE J Sel Top Appl Earth Obs Remote Sens*, vol. 8, no. 6, pp. 3224–3234, 2015.